ELSEVIER

Chemical Geology 138 (1997) 221–244

CHEMICAL GEOLOGY
INCLUDING
ISOTOPE GEOSCIENCE

SIMS analysis of oxygen isotopes: matrix effects in complex minerals and glasses

John M. Eiler [a,*], Colin Graham [b], John W. Valley [c]

[a] *Division of Geological and Planetary Sciences, California Institute of Technology, Pasadena, CA 91125, USA*
[b] *Department of Geology and Geophysics, University of Edinburgh, Edinburgh, EH9 3JW, Scotland, UK*
[c] *Department of Geology and Geophysics, University of Wisconsin, Madison, WI 53706, USA*

Received 9 December 1996; accepted 4 February 1997

Abstract

A large instrumental mass fractionation (IMF) occurs during the measurement of oxygen isotope ratios by secondary ion mass spectrometry and the magnitude of this fractionation can be dependent upon sample chemistry, resulting in so-called 'matrix effects'. We have made 373 measurements of the $^{18}O^-/^{16}O^-$ ratio (± 0.5–$1.1‰$ internal precision, 1 s.d.) in 40 silicate and phosphate minerals and glasses for the purpose of characterizing this matrix effect. The magnitude of IMF decreases with increasing atomic mass of the sample, although this relationship is too poorly defined to be the basis of a precise empirical correction scheme. IMF is well correlated with simple measures of chemistry among related minerals and glasses (e.g. forsterite content in olivine; Na/(Na + K) in feldspathic glass), and with the atomic abundance of certain elements among several mineral groups (e.g. the sum: (Fe + Mn) in garnets, olivines and pyroxenes). Significant differences in IMF between minerals and glasses of the same chemical composition correlate with the mass of network *modifying* cations. Instrumental mass fractionation correlates strongly with sputter rate for albite and seven silicate glasses.

Two mechanisms for producing matrix effects are proposed: (1) differences in the efficiency with which kinetic energy is transferred to the secondary oxygen atoms from the atoms in the near-surface region of the sample, and (2) simple variations in the fraction of sputtered oxygen atoms that are ionized, such that the observed instrumental fractionation diminishes as that fraction approaches 1. The correlation between sputter rate and instrumental mass fractionation in silicate glass and albite is well predicted by model (1). Our data suggest that a large range of silicate materials can be standardized using: (1) interpolation among chemically similar standards; (2) correlation of IMF with Fe + Mn content in materials rich in those elements; (3) model (1), particularly for materials that are compositionally related to standards

One or more of these methods appear to be applicable to most silicate materials of interest and should permit accurate standardization of ion probe analyses without the stringent requirements that standards and unknowns be compositionally identical or compositionally similar members of the same solid solution series.

Keywords: Ion microprobe; Oxygen isotopes; Matrix effects; Standards

1. Introduction

Considerable effort has been made over the last decade to develop precise and accurate methods for

* Corresponding author.

0009-2541/97/$17.00 Copyright © 1997 Elsevier Science B.V. All rights reserved.
PII S0009-2541(97)00015-6

the analysis of the isotopic ratios of oxygen in natural materials by secondary ion mass spectrometry (SIMS) (McKeegan, 1987; Lorin et al., 1990; Valley and Graham, 1991; Hervig et al., 1992; Riciputi and Paterson, 1994; Valley and Graham, 1996; see Valley et al., 1997a). Such efforts are justified by the great advantages of an in-situ technique with micron (μm) spatial resolution, which permits the measurement of isotopic compositions of very small samples or of inter- and intra-crystalline zonation in larger samples. To some extent, these are also the goals of recently developed methods of laser-aided fluorination of small silicate and oxide samples (Sharp, 1990; Elsenheimer and Valley, 1992; Mattey and Macpherson, 1993; Valley et al., 1995; Wiechert and Hoefs, 1995). However, the ion microprobe is currently the only technique with an effective spatial resolution on the scale of a few μm, and is therefore uniquely suited to many analytical problems. For example, the smallest samples that have been analyzed for oxygen isotope composition by a fluorination-based technique are 20 μg (Mattey and Macpherson, 1993), and the practical limit without corrections for fractionation of gases is >200 μg (Mattey and Macpherson, 1993; Valley et al., 1995). A typical ion probe analysis consumes 0.005–0.010 μg of sample (Valley et al., 1997a). Methods of light isotope analysis by carrier gas entrainment followed by gas-chromatography and mass spectrometry (Ricci et al., 1994) have sample sizes approaching those of typical ion microprobe analyses with precision of ~ 0.2–0.5‰, but have not been successfully coupled with a micro-sampling technique for minerals for sample sizes smaller than ~ 20 μg (Sharp and Cerling, 1995).

Initial studies showed the SIMS technique for electrically insulating samples (e.g. silicates) to be hampered both by imprecision (± 3–5‰ for $^{18}O/^{16}O$, 1 s.d.), due to low count rates and instabilities in the charge of the sample during and among analyses, and by inaccuracies caused by variable instrumental mass fractionations (IMF) (McKeegan, 1987; Giletti and Shimizu, 1989; Lorin et al., 1990; Yurimoto et al., 1994). These levels of accuracy and precision permitted the study of meteoritic samples, in which oxygen isotope variations can be large (McKeegan, 1987), but initially ruled out the meaningful analysis of terrestrial samples, most of which span only a 10–15‰ range in $^{18}O/^{16}O$. Precisions have been significantly improved in recent years due to innovations such as the use of the normal-incidence electron 'flood gun', the adoption of a technique in which only secondary ions with initial kinetic energies greater than 300 eV are analyzed (energy filtering), and more common use of short (~ 15 ns) dead-time electron multiplier counting systems for this work. Internal and point-to-point precisions are now routinely 1.0‰, and sometimes as good as 0.4‰, 1 s.d. (Hervig et al., 1992; Riciputi and Paterson, 1994; Valley and Graham, 1996; Valley et al., 1997b; this study). While precisions are approaching those of fluorination-based analyses, accuracies remain poor if standards are not chemically identical to unknowns due to IMF being dependent upon sample properties.

1.1. Matrix effects and the standardization of SIMS analysis

The principal limitation of SIMS analysis of geological materials is the strong instrumental fractionation of elemental and isotopic compositions (Shimizu and Hart, 1982 and references therein). There are several sources of instrumental fractionation, including secondary atom extraction (sputtering) and ionization (Sigmund, 1969; Shroeer et al., 1973; Williams, 1979; Yu and Lang, 1986), secondary ion transmission (Shimizu and Hart, 1982), and detection (discussed with reference to oxygen isotope analysis by Valley and Graham, 1991 and Lyon et al., 1994). The latter two processes do not vary from sample to sample, and can therefore be relatively easily corrected for. Fractionation during sputtering/ionization is more complex, and is to some degree dependent upon sample properties. Isotopic fractionations in single-element samples (e.g. Slodzian et al., 1980; Shimizu and Hart, 1982; Weathers et al., 1993) and chemical fractionations in more complex, polyatomic, compounds (Deline et al., 1978; Shimizu and Hart, 1982) are well documented, and qualitatively explicable by secondary ion production theory. However, the physics underlying matrix effects in the isotopic analysis of complex materials such as silicates is relatively unknown. The isotopic matrix effect has been carefully explored for D/H ratio measurements in amphiboles and micas (Deloule et

al., 1991), revealing a correlation with major element chemistry. The first-order correlation between instrumental mass fractionation of D/H and specific chemical parameters that are also predictive of mineral–water equilibrium isotopic fractionations was taken as an indication that the matrix effect is in this instance controlled by the local bonding environment of hydrogen in hydrous minerals.

Some studies of oxygen isotope ratios measured by SIMS found no significant differences in instrumental mass fractionation among some silicate and oxide phases (McKeegan, 1987; Lorin et al., 1990; Yurimoto et al., 1994; Leshin et al., 1996). However, the analytical conditions with which these data were collected differed from the emphasis on high-energy secondary ions common to recent work, external precision of some of these data were as poor as ±3–5‰ (1 s.d.) and the suite of standards was relatively restricted, reducing the general significance of these results. However, matrix effects were also observed to be essentially absent in the isotopic analysis of some binary alloys, revealing a general trend that SIMS analysis fractionates isotopes as a simple function of their mass ratio (Slodzian et al., 1980; Shimizu and Hart, 1982). These results suggested that instrumental mass fractionations for high-precision oxygen isotope analysis in silicates might not require mineral-specific and/or compositionally dependent corrections.

More recent detailed studies of oxygen isotope analysis by SIMS have revealed significant matrix effects and suggested two different approaches to the problem of standardization. Hervig et al. (1992) present an empirical correction for the matrix effect, based on data for quartz, clinopyroxene, several forsteritic olivines, and magnetite. Hervig et al. found that for secondary ions sputtered with high initial kinetic energies (300 + eV), values of IMF for these minerals are correlated with formula weight (normalized to a constant number of oxygens). This correlation is best when considering only the data for silicate minerals. This is an extremely useful result if correct, for it would mean that even minerals that are only distantly related to standards (e.g., both being silicates) can be analyzed with an accuracy nearly approaching measurement precision simply by applying an empirical correction based on the formula weight of the unknown. Such a simple matrix correction was used to compare the isotopic compositions of different portions of chemically zoned garnets (Jamtveit and Hervig, 1994). Subsequently, this approach has been called into question. In a study comparing IMF among quartz, albite, orthoclase, clinopyroxene, calcite, and several garnets of variable chemical composition, Riciputi and Paterson (1994) found that the simple correlation proposed by Hervig et al. (1992) was violated by > 10‰, suggesting that matrix effects cannot be inferred from analysis of chemically dissimilar standards using this algorithm.

The fundamental problem underlying these apparently contradictory results is the absence of any clearly identified physical mechanisms which might contribute to the matrix effect. In this paper we present 373 SIMS analyses of the $^{18}O/^{16}O$ ratio in 40 silicate and phosphate minerals and glasses in an effort to characterize the matrix effect, to constrain the mechanisms by which it may be produced, and to create a reliable correction procedure applicable to minerals with complex chemical formula.

2. Analytical technique

All analyses reported in this study were made on the Cameca ims–4f™ ion microprobe at the University of Edinburgh, Scotland, between Dec. 4, 1995 and Dec. 22 1996. General procedures are reviewed elsewhere (Valley et al., 1997a). Measurements were made with a (~ 8 nA, 14.15 keV) primary beam of magnetically filtered $^{133}Cs^+$ ions, focused to a 20–30 μm spot. A normal-incidence electron 'flood gun' was used to provide charge compensation during analysis. Secondary ions were accelerated by 4.15 keV and electrostatically analyzed to accept those emitted with excess energies of 350 ± 26 eV. Secondary $^{18}O^-$ and $^{16}O^-$ ions were alternately measured by magnetic peak switching on an ETP™ electron multiplier with an ECL counting system. Count rates were typically ~ 10^6 cps of ^{16}O and ~ $2 \cdot 10^4$ cps of ^{18}O. Dead-time corrections were made using the measured deadtime of 14 ns for the counting system, determined immediately prior to each 1–2 week period of analysis. Each analysis represents 120 cycles comparing 1-s measurement of mass 16 and 5-s measurement of mass 18, with a

magnet settling time of 50 ms between peaks. Some analyses were made with 200 cycles (counts of 1 and 10 s, respectively) in order to assess the limits of within-run precision and the effect of count-time on measured isotopic compositions. Expected theoretical precisions for these count rates and times were approximately ±0.9‰ for most analyses, and ±0.5‰ for 200-cycle analyses, simply based on counting statistics of the total number of ^{18}O counts. Actual internal precision (i.e. the standard error of the population of 120 or 200 cycles) averaged ±0.92‰ for shorter analyses and ±0.60‰ for longer, indicating that internal errors due to within-run instabilities or other analytical factors were a minor contribution to the overall precision. Point-to-point reproducibilities of repeated analyses of nominally homogeneous materials averaged ±0.75‰ for short analyses and ±0.52‰ for long counting times, also indicating that there was little or no uncertainty introduced to the total analytical precision beyond that inherent in the counting statistics of each analysis.

Analyses have been organized chronologically into nineteen blocks, separated by sample changes and/or major instrumental changes, such as major re-focusing of the primary beam or electron flood gun, or change in the electron multiplier gain. Sixteen of these nineteen blocks showed no evidence of internal 'drift' (i.e. monotonic change in the measured isotopic composition of standards with time). The blocks which did show clear evidence of internal drift have been corrected by regressing data for the most frequently analyzed sample as a function of analytical order, and correcting all data for that block according to the resulting slope (these blocks are indicated in Table 2). In these blocks, drift was approximately 0.1‰ per analysis. It has been hypothesized that drift results from degradation of the electron multiplier (Valley and Graham, 1991; Eiler et al., 1995; Valley et al., 1997a). Two observations from this study support this hypothesis: (1) the dependence of count rate upon electron multiplier voltage was monitored frequently throughout this work and was seen to shift steadily over periods of days to weeks; (2) the electron multiplier voltage was raised by ~50 eV after analytical blocks in which drift was observed, and no drift was observed in the following block. Rarely, a single analysis deviated by a large amount from all other analyses of the same material (by more than 3 s.d. from the average) for an unknown reason, which could include real heterogeneities in the samples. In these instances that analysis was culled as an outlier. Only two analyses out of 373 were removed from the data base for this reason.

3. Samples

The suite of materials analyzed in this study includes 25 silicate minerals, 13 silicate glasses, and 2 apatites (Table 1). All were either analyzed for major element content by electron microprobe, or are essentially invariant in their chemistry and are assumed to have an end-member composition (e.g. quartz). All but two of the silicate minerals and glasses were analyzed for oxygen isotopic composition by laser fluorination at the University of Wisconsin (techniques described by Valley et al., 1995). Of these analyses, 32 were replicated with an average reproducibility of ±0.07‰. Six of these (three minerals and three glasses) were also analyzed by conventional, resistance-heated fluorination in several independent laboratories, with an average agreement between the two techniques of ±0.08‰. One garnet (UWG-2) was analyzed multiple times in seven conventional and laser-fluorination laboratories, with all labs agreeing to within ±0.1‰ (Valley et al., 1995). Both fluor-apatites were analyzed by conventional fluorination (Farqhar et al., 1993; Santos and Clayton, 1995). One pyroxene (87G pyroxene) was analyzed by conventional fluorination at the University of Monash, Australia. Values for zircons (Kim-2 and Jwan) are reported in Valley et al., 1997b.

Fragments of minerals and glasses were prepared by gently breaking samples in a steel percussion mortar, and were mounted with Buehler™ epoxy into 2 mm holes drilled into 2.5 cm diameter aluminum metal disks suitable for insertion into a commercial Cameca™ sample holder. Each disk was then hand-polished down to 0.03 μm alumina grit, ultrasonically cleaned in ethanol, and stored in a plastic box until analysis. Each sample holder can contain up to 20 samples, and sufficient repetition of samples between multiple holders was made to allow direct comparisons among a large subset of the

Table 1
Samples analyzed for $^{18}O/^{16}O$ by SIMS

Sample	Composition	$\delta^{18}O$	$^{18}O/^{16}O$	Mean atomic mass (AMU)
Framework silicates				
Hot Springs quartz	SiO_2	10.6	0.0020265	20.03
Brazil quartz	SiO_2	9.6	0.0020244	20.03
Amelia albite	$NaAlSi_3O_8$	10.8	0.0020268	20.17
P490 orthoclase	$KAlSi_3O_8$	7.9	0.0020210	21.41
Garnets				
UWG-2 garnet	$(Ca_{.13}Mg_{.39}Fe_{.47}Mn_{.01})_3Al_2Si_3O_{12}$	5.8	0.0020168	22.73
Spessartine garnet	$(Fe_{.05}Mn_{.95})_3Al_2Si_3O_{12}$	5.4	0.0020160	24.80
Pyrope garnet	$(Ca_{.12}Fe_{.13}Mg_{.75}Mn_{.02})_3(Al_{.88}Fe_{.04}Cr_{.07})_2Si_3O_{12}$	6.0	0.0020172	21.39
Almandine SE garnet	$(Ca_{.01}Mg_{.25}Fe_{.74})_3Al_2Si_3O_{12}$	8.3	0.0020218	23.68
Almandine CMG gaMet	$(Ca_{.03}Mg_{.25}Fe_{.70}Mn_{.02})_3Al_2Si_3O_{12}$	7.5	0.0020202	23.66
Grossular garnet	$(Ca_{.98}Mn_{.02})_3(Al_{.97}Fe_{.03})_2Si_3O_{12}$	3.8	0.0020128	22.65
Chain silicates				
UWW-1 wollastonite	$CaSiO_3$	0.1	0.0020053	23.23
JV1 diopside	$CaMg_{.93}Fe_{.07}Si_2O_6$	20.3	0.0020459	21.90
Jadeite	$NaAlSi_2O_6$	9.4	0.0020239	20.21
Enstatite-1	$Mg_{.87}Fe_{.13}SiO_3$	9.2	0.0020236	20.90
87G pyroxene	$CaMg_{.44}Fe_{.66}Si_2O_6$	8.1	0.0020214	23.74
Olivine				
Fay 50278 olivine	$(Mg_{.006}Fe_{.994})_2SiO_4$	4.5	0.0020142	29.06
Pit-16 olivine	$(Mg_{.752}Fe_{.248})_2SiO_4$	5.3	0.0020159	22.34
Pit-7 olivine	$(Mg_{.737}Fe_{.263})_2SiO_4$	5.3	0.0020158	22.47
R142–1.60 olivine	$(Mg_{.864}Fe_{.136})_2SiO_4$	5.4	0.0020160	21.33
R160–5.75 olivine	$(Mg_{.858}Fe_{.142})_2SiO_4$	4.9	0.0020150	21.38
R303–3.0 olivine	$(Mg_{.858}Fe_{.142})_2SiO_4$	4.7	0.0020147	21.38
R243–8.40 olivine	$(Mg_{.877}Fe_{.123})_2SiO_4$	4.6	0.0020145	21.21
San Carlos olivine	$(Mg_{.903}Fe_{.097})_2SiO_4$	5.3	0.0020157	20.98
Zircon				
Kim-2 zircon	$ZrSiO_4$	5.6	0.0020164	30.55
Jwan zircon	$ZrSiO_4$	4.7	0.0020146	30.55
Phosphate				
Jacapuranga apatite	$Ca_5(PO_4)_3F$	4.6	0.0020144	24.01
Laramie apatite	$Ca_5(PO_4)_3F$	7.3	0.0020198	24.01
Glasses				
HSQ glass	SiO_2	10.8	0.0020268	20.03
Na–Mel glass	$Na_{1.2}Ca_{1.1}Al_{1.2}Si_{2.3}O_8$	11.6	0.0020285	21.46
Albite glass	$NaAlSi_3O_8$	10.8	0.0020268	20.17
Jadeite glass	$NaAlSi_2O_6$	12.7	0.0020307	20.21
Anorthite glass	$CaAl_2Si_2O_8$	8.3	0.0020218	21.40
Ab–Or glass	$K_{.52}Na_{.48}AlSi_3O_8$	14.8	0.0020349	20.82
Or glass	$KAlSi_3O_8$	10.3	0.0020259	21.41
Ab7, hydrous Ab glass	$(NaAlSi_3O_8)_{.48}(H_2O)_{.52}$	3.1	0.0020113	17.30
UWG-2 garnet glass	$(Ca_{.13}Mg_{.39}Fe_{.47}Mn_{.01})_3Al_2Si_3O_{12}$	5.8	0.0020168	22.73
Glass Butte rhyolite	77.5 wt% SiO_2	7.3	0.0020198	20.48
519-4-1 basalt	48.69 wt% SiO_2; 8.79 wt% FeO	5.2	0.0020156	21.78
MK1-8 basalt	52.52 wt% SiO_2; 10.59% FeO	5.0	0.0020152	21.76
AH95-22 basalt	50.82 wt% SiO_2; 11.02 wt% FeO	4.9	0.0020151	21.91

Assumes $^{18}O/^{16}O = 0.00200520$ in standard mean ocean water (SMOW), Baertschi (1976) and that $\delta^{18}O$(NBS-28) = 9.59‰ relative to SMOW.

specimens without a sample change. Samples were coated with Au and a Ag colloid paint applied to the edges of each sample prior to insertion into the specimen chamber of the Cameca ims-4f.

4. Results

Data are reported in Table 2 as the average measured $^{18}O/^{16}O$ ratio and the average instrumental mass fractionation expressed as an alpha ratio:

$$\alpha_{SIMS} = {}^{18}O/{}^{16}O_{measured}/{}^{18}O/{}^{16}O_{actual} \quad (1)$$

In addition, the IMF is reported in units of permil, calculated by the relationship:

$$IMF = \left(\left({}^{18}O/{}^{16}O_{measured} - {}^{18}O/{}^{16}O_{actual}\right) / {}^{18}O/{}^{16}O_{actual}\right) \cdot 1000 \quad (2)$$

The average and standard error (point-to-point precision, 1 standard deviation (s.d.), divided by $n^{1/2}$) are reported for this second measure of IMF. The number of analyses of each material in each block, n, is reported. The ratio: $^{18}O/^{16}O_{measured}$ includes dead-time correction and culling of 3σ outliers to the population of 120 or 200 cycles, and $^{18}O/^{16}O_{actual}$ assumes a value of $2.00520 \cdot 10^{-3}$ for standard mean ocean water (Baertschi, 1976). The conversion of results to deviations in units of permil by Eq. (2) was made to conform to standard stable isotope notation. An error would be introduced by applying these fractionations to materials with significantly different values of $^{18}O/^{16}O_{actual}$.

The seventeen blocks of data in which more than one mineral is compared have been mutually normalized by the following algorithm. The instrumental mass fractionations in the eleven blocks in which Amelia albite was analyzed were normalized to a constant value for this material (equal to the average of all observed values). The four remaining blocks (1, 10, 11, and 15) were normalized to the others by correction to the value for San Carlos olivine, JV-1 diopside or UWG-2 observed in the eleven mutually normalized blocks. This normalization was made to remove the effects of IMF caused by non-sample-related phenomena (e.g. changes in the electron multiplier voltage), allowing us to observe differences related only to matrix effects. The normalization is relatively small; day-to-day variations in the observed IMF for Amelia albite averaged 3‰ for seventeen blocks over a one-year period (total range 11.3‰). Normalization was made by multiplying the measured $^{18}O/^{16}O$ ratio of all materials in a block by α_{SIMS}, defined as the ratio $(^{18}O/^{16}O)_{measured}/(^{18}O/^{16}O)_{standard}$, where the 'standard' value is the normalized value for a reference material (e.g. average Amelia albite for most blocks). Given the ± 0.3‰ (1σ) average uncertainty in IMF for the reference materials on any given day, this normalization should introduce little uncertainty in comparing IMF of materials from different sessions. One measure of the success of this method of mutual normalization is the reproducibility of normalized fractionations between different analytical blocks. Reproducibility averaged ± 0.49‰ for five different materials (Ab7, three separate blocks; Or glass, Ab glass, Jadeite glass and enstatite, two blocks each), comparable to the average standard error for each individual measurement (± 0.53‰). This demonstrates that differences between the fractionations of different samples are independent of day-to-day variations in the raw, pre-normalization fractionation over the range observed in this study. Data for two additional blocks are given in Table 2 (blocks 13 and 14) which were not used in the study of matrix effects, one comparing long and short analytical times in JV-1 diopside, and the other comparing raw measured isotopic compositions in two crystallographic orientations of quartz. No normalization was made for these blocks.

The instrumental mass fractionations observed in this study are all negative as defined by Eq. (2), conforming to the general observation that SIMS measurements discriminate against heavy isotopes under most analytical conditions in most materials (Slodzian et al., 1980; Shimizu and Hart, 1982). The total range in average instrumental mass fractionations (prior to normalization) was from -30.3 to -74.7‰, comparable to that observed in previous studies which measured only relatively high-energy (≥ 300 eV) secondary ions (Hervig et al., 1992; Riciputi and Paterson, 1994; Valley and Graham, 1996; Graham et al., 1996). These fractionations are much larger than those observed in the analysis of low-energy secondary ions (e.g. -19 to -30‰ on magnetite; Valley and Graham, 1991), an observation that runs contrary to the inverse dependence of

mass fractionations on secondary ion velocity seen at low energy (Gnaser and Hutcheon, 1987) and perhaps indicates a different ionization mechanism for high-energy secondary ions (Schauer and Williams, 1990; Hervig et al., 1992). However, comparison with analysis of low-energy secondary ions is further complicated by the fact that most such data was measured on electrically conductive minerals, whereas most analyses of high-energy secondary ions have been of electrically insulating minerals.

Several general correlations were observed between a sample's normalized fractionation and other properties. These are described in the following sections in order of increasing complexity.

4.1. Minerals

The average instrumental mass fractionations among our 26 minerals for which mutual normalizations were made, demonstrate a significant correlation between IMF and mean atomic weight (Fig. 1A). The data define a positive slope, such that materials rich in high-AMU cations are relatively unfractionated. The overall correlation is poor, but subdivision of the data by composition suggests systematic behavior among large subsets of the data. For example, all calcium-rich phases (unfilled symbols) fall below the trend defined by calcium-poor phases, and all calcium-poor phases other than zircon (18 minerals) fall within 1.5‰ of a single curve (most are within 1‰ of this curve). Further subdivision of framework silicates, olivines, etc. also permits the definition of mineral-specific trends that are well defined. However, the overall correlation for all data is violated by up to 6.5‰, making this relationship unsuitable as the basis for a general empirical correction scheme. The correlation in Fig. 1A is similar to that observed when plotting IMF vs. the formula weight normalized to a constant number of oxygens (e.g., Hervig et al., 1992; Riciputi and Paterson, 1994).

Correlations are observed between IMF and simple measures of chemistry among related minerals, such as mole fractions of solid solution end members. The best examples of this are data for olivines. Olivines with atomic ratios of Mg/(Mg + Fe) ($\equiv X_{Fo}$) of between 0.91 and 0.006 were analyzed, and found to have a regular dependence of IMF on X_{Fo} (Fig. 2). The slope to the Mg-rich end of this trend is indistinguishable from that observed in magnesian olivines by Riciputi and Paterson (1997). This correlation is important in two regards: (1) it is a relatively simple relationship that should permit stan-

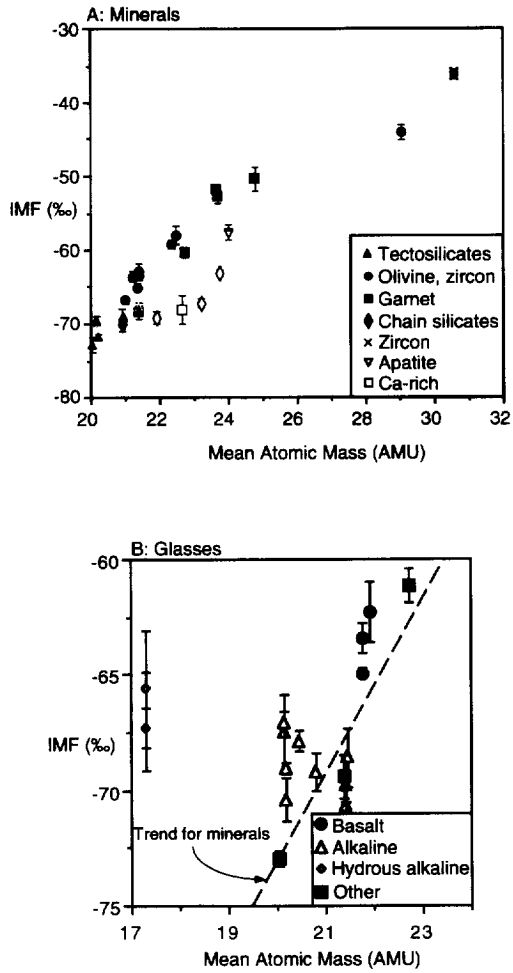

Fig. 1. Measured instrumental mass fractionations (IMF) for SIMS analysis of minerals and glasses in units of permil deviation from actual $^{18}O/^{16}O$ ratios (see text Eq. (2)). All data normalized to constant value for Amelia albite (Table 2). Most data for silicate and phosphate minerals (A) and silicate glasses (B) define an approximately linear trend of smaller fractionations with increasing mean atomic mass. Deviations from this are up to 6.5‰, many times analytical uncertainty (plotted as 2σ of the mean, i.e. 2 s.d./$n^{1/2}$), indicating confounding variables and/or the incorrect choice of correlatives to describe the matrix effect. Subsets of minerals show better correlation than is seen in the data as a whole; e.g. Ca-rich minerals (open symbols) are systematically below Ca-poor minerals (filled symbols).

Table 2
SIMS measurements of oxygen isotope ratios

Block	Sample	$^{18}O/^{16}O$ [a]	α_{SIMS} [b]	IMF (‰) [c]	Normalized IMF (‰) [d]	n
1	JV diopside	0.0019112	0.93415	−65.85 ± 0.60	**−69.16**	4
	Fayalite	0.0019319	0.95914	−40.86 ± 0.51	**−44.26**	5
	Pit-16	0.0019033	0.94413	−55.87 ± 0.29	**−59.21**	5
	Pit-7	0.0019056	0.94530	−54.70 ± 0.61	**−58.05**	7
	R160	0.0018950	0.94048	−59.52 ± 0.47	**−62.85**	7
	R243	0.0018931	0.93972	−60.28 ± 0.32	**−63.61**	7
	R303	0.0018933	0.93977	−60.23 ± 0.29	**−63.56**	5
	R142	0.0018916	0.93829	−61.71 ± 0.24	**−65.03**	5
	San Carlos	0.0018877	0.93650	−63.50 ± 0.27	**−66.82**	15
2 [f]	Amelia albite	0.0018906	0.93282	−67.18 ± 0.18	**−69.64**	8
	Hot Springs quartz	0.0018839	0.92963	−70.37 ± 0.50	**−72.82**	6
	P490 orthoclase	0.0018893	0.93480	−65.20 ± 0.24	**−67.67**	3
	San Carlos olivine	0.0018860	0.93565	−64.35 ± 0.49	**−66.82**	2
	HSQ glass	0.0018839	0.92952	−70.48 ± 0.17	**−72.93**	3
	Albite glass	0.0018958	0.93533	−64.67 ± 0.25	**−67.14**	3
3	Amelia albite	0.0018846	0.92986	−70.14 ± 0.45	**−69.64**	6
	Orthoclase glass	0.0018816	0.92879	−71.21 ± 0.11	**−70.71**	3
	Jadeite	0.0018776	0.92771	−72.29 ± 0.22	**−71.79**	3
	Jadeite glass	0.0018867	0.92910	−70.90 ± 0.46	**−70.40**	3
	UWG-2 garnet	0.0018940	0.93911	−60.89 ± 0.31	**−60.38**	13
	UWG-2 glass	0.0018926	0.93838	−61.62 ± 0.37	**−61.12**	5
4	Amelia albite	0.0018817	0.92841	−71.59 ± 0.36	**−69.64**	3
	Albite glass	0.0018860	0.93051	−69.49 ± 0.85	**−67.54**	1
	AB7 glass	0.0018720	0.93071	−69.29 ± 0.88	**−67.34**	1
5	Amelia albite	0.0018863	0.93066	−69.34 ± 0.02	**−69.64**	2
	AB7 glass	0.0018799	0.93467	−65.33 ± 1.28	**−65.63**	1
6	Amelia albite	0.0018893	0.93218	−67.82 ± 0.22	**−69.64**	3
	Jadeite glass	0.0018942	0.93280	−67.20 ± 0.12	**−69.02**	2
7	Amelia albite	0.0018828	0.92893	−71.07 ± 0.26	**−69.64**	9
	Orthoclase glass	0.0018817	0.92881	−71.19 ± 0.58	**−69.76**	4
	Ab–Or glass	0.0018911	0.92933	−70.67 ± 0.41	**−69.24**	3
	An glass	0.0018787	0.92919	−70.81 ± 0.47	**−69.38**	4
	Na–melilite glass	0.0018865	0.92999	−70.01 ± 0.64	**−68.58**	5
8	Amelia albite	0.0018772	0.92620	−73.80 ± 0.64	**−69.64**	6
	AB7 glass	0.0018709	0.93019	−69.81 ± 0.38	**−65.63**	3
9 [f]	Amelia albite	0.0018927	0.93383	−66.17 ± 0.26	**−69.64**	11
	Glass Butte rhyolite	0.0018897	0.93560	−64.40 ± 0.21	**−67.88**	3
	AH95-22	0.0018966	0.94121	−58.79 ± 0.66	**−62.29**	3
	519-4-1	0.0018917	0.93853	−61.47 ± 0.11	**−64.96**	3
	MK1-8	0.0018943	0.94003	−59.97 ± 0.32	**−63.46**	2
10	JV diopside	0.0018975	0.92747	−72.53 ± 0.29	**−69.16**	3
	Laramie apatite	0.0018963	0.93885	−61.15 ± 0.14	**−57.74**	3
	Jacapuranga apatite	0.0018918	0.93912	−60.88 ± 0.48	**−57.47**	3

Table 2 (continued)

Block	Sample	$^{18}O/^{16}O$ [a]	α_{SIMS} [b]	IMF (‰) [c]	Normalized IMF (‰) [d]	n
11	JVdiopside	0.0019079	0.93256	−67.44 ± 0.36	**−69.16**	6
	UWW-1 wollastonite	0.0018742	0.93462	−65.38 ± 0.33	**−67.10**	12
12	UWG-2 garnet	0.0018915	0.93786	−62.14 ± 0.53	**−60.38**	9
	Spessartine	0.0019110	0.94788	−52.12 ± 0.83	**−50.35**	5
	Pyrope	0.0018756	0.92978	−70.22 ± 0.45	**−68.48**	9
	Almandine SE	0.0019116	0.94547	−54.53 ± 0.45	**−52.76**	2
	Almandine CMG	0.0019118	0.94634	−53.66 ± 0.39	**−51.89**	3
	Grossular	0.0018722	0.93016	−69.84 ± 1.00	**−68.10**	1
13 [e f]	Quartz, parallel C	0.0018739	0.92562	−74.38 ± 0.34	–	10
	Quartz, perpendicular C	0.0018732	0.92529	−74.71 ± 0.19	–	15
14	JV diopside, short counts	0.0019078	0.93250	−67.50 ± 0.44	–	3
	JV diopside, long counts	0.0019079	0.93255	−67.45 ± 0.17	–	10
15	JV diopside	0.0019066	0.93191	−68.08 ± 0.36	**−69.16**	10
	87G pyroxene	0.0018962	0.93805	−61.95 ± 0.23	**−63.02**	17
17	Amelia albite	0.0018940	0.93448	−65.52 ± 0.60	**−69.64**	11
	Enstatite-1	0.0018906	0.93430	−65.70 ± 0.26	**−69.83**	8
18	Amelia albite	0.0019002	0.93754	−62.46 ± 0.36	**−69.64**	3
	Enstatite-1	0.0018975	0.93767	−62.33 ± 0.75	**−69.51**	3
19	Amelia albite	0.0018971	0.93601	−63.99 ± 0.59	**−69.64**	11
	Kim-2 zircon	0.0019548	0.96944	−30.56 ± 0.29	**−36.42**	13
	Jwan zircon	0.0019536	0.96969	−30.31 ± 0.38	**−36.17**	14

[a] Average value of n analyses. Reproducability given in units of permil under IMF.
[b] $\alpha_{SIMS} = {}^{18}O/{}^{16}O$ (measured)/$^{18}O/^{16}O$ (actual).
[c] Calculated using Eq. 2.
[d] Corrected for day-to-day shifts in a reference standard (see text).
[e] Sputter rates for these two orientations were indistinguishable.
[f] Drift correction applied to block.
Uncertainties are 1σ in the mean of n measured points. Minimum total uncertainties cannot be less than $1/n^{0.5}$ for most of these measurements.

dardization by interpolation with sufficient data on standards; but (2) it is significantly non-linear, indicating that mineral-specific corrections based on the linear calibration of solid solution series are unsuitable for significant extrapolation, and may not be safely applied to extensive interpolation (e.g. there is a 5‰ deviation of data for $X_{Fo} \sim 0.70$ from a line between $X_{Fo} = 0.906$ and $X_{Fo} = 0.006$). The non-linearity in Fig. 2 is similar to the curve for non-calcic minerals in Fig. 1A, where the same non-linearity defined in part by olivine is shared by Fe–Mg–Mn garnets, enstatite, and the framework silicates.

Finally, matrix effects are highly correlated with the abundance of certain major elements in minerals that contain a significant amount of that element. This is illustrated in Fig. 3, where the IMF for sub-sets of the silicate minerals are plotted vs. the mole fractions of (Fe + Mn) and Ca in minerals rich in those elements. Both trends are free of mineral-specific differences. Variations in IMF with Na, K and Al content in the alkaline feldspars and pyroxenes are defined by only 1–2 points, but are also shown for comparison. The trends for both (Fe + Mn) and Ca define lines that have Y intercepts approximately equal to the IMF for SiO_2. The trend of IMF

vs. (Fe + Mn) content is particularly significant in that it is composed of 15 different points from 3 different mineral groups (5 garnets, 8 olivines and 2 pyroxenes). This trend is comparable to that observed between IMF and mean atomic weight in Ca-poor minerals.

While subdivision of the data by mineral groups can lead to well defined correlations (e.g., Fig. 2), this appears to be unnecessary on the basis of correlations with the absolute abundance of certain elements among multiple mineral groups (e.g. Fig. 3). Therefore, our results suggest that matrix effects are element-specific rather than mineral-specific. There is an apparent progression in the sensitivity of IMF to different elements, such that small-radius, heavy elements (Fe, Mn, Zr) exert a much stronger apparent influence than do large-radius, moderately heavy elements (Ca, K), which exert a somewhat stronger influence than light elements (Na, Al, and Si as represented by quartz).

Two minerals that are essentially identical in their chemistry and structure (Kim-2 and Jwan zircons) yielded values of IMF that are the same within 1σ precision (Table 2), supporting the implicit assumption of this and previous studies that minor differences in structure and/or chemistry likely have no effect on IMF.

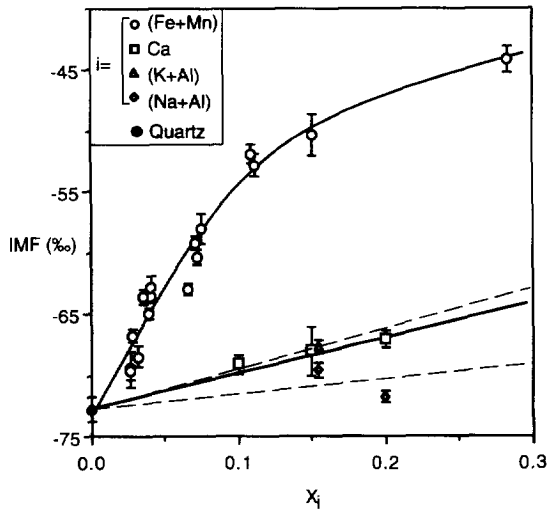

Fig. 3. Correlations between IMF and mole fractions of various elements in silicate minerals. Data are subdivided into four groups: $X_{Fe} + X_{Mn}$ in all minerals containing > 1% Fe and/or Mn (including olivines, garnets, and pyroxenes), X_{Ca} in minerals rich in Ca (wollastonite, diopside, grossular). We have also plotted data vs. $(X_{Na} + X_{Al})$ or $(X_K + X_{Al})$ in albite, jadeite and orthoclase for comparison. All sets of points are joined by lines to quartz, which is free of all of the listed components and is a shared major constituent in all of the phases. IMF varies regularly with abundances of certain elements, irrespective of the phase in which it is present, and the sensitivity of IMF to abundance differs substantially among the elements. These observations suggest that IMF may be empirically fit based upon elemental compositions. Error bars are 2σ uncertainty in the mean.

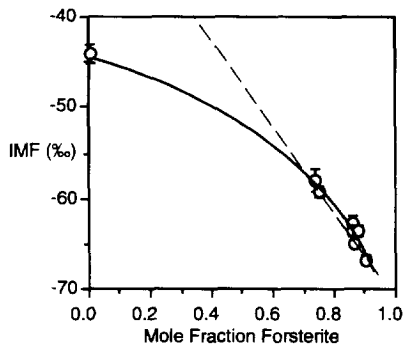

Fig. 2. Values of IMF for olivines plotted against the mole fraction of forsterite (Mg/(Mg+Fe)). The correlation among forsteritic olivines is approximately linear (dashed line) and has a slope equal to that recently obtained in another laboratory (Riciputi and Paterson, 1997). The correlation must, however, be highly non-linear over its full length, since fayalite deviates from the extension of that straight line by 20‰. Error bars are 2σ uncertainty in the mean.

4.2. Glasses

The eighteen independent measurements of instrumental mass fractionation for thirteen different glasses are generally concordant with the line defined in Fig. 1A for minerals, although the deviation from this trend, even excluding the clear exception of hydrous albite, are greater than analytical uncertainty (up to 5‰; Fig. 1B). Hydrous albite strongly violates this trend, having approximately the same instrumental mass fractionation as the anhydrous albite glass and crystalline albite, despite a much lower mean atomic mass. Otherwise, the least well-correlated samples in Fig. 1B are the alkaline glasses, which scatter to points both above and below the average trend for minerals.

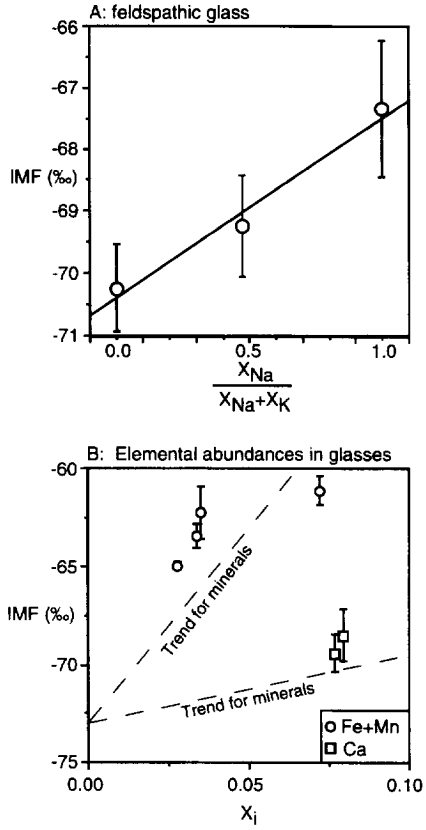

Fig. 4. Values of IMF for subsets of the silicate glass samples, plotted against major chemical indices: (A) mole fraction albite, 'X_{Ab}', in alkali feldspar glasses; (B) $X_{Fe} + X_{Mn}$ and X_{Ca} in glasses rich in those elements. As with minerals, correlations between fractionation and major element contents among related glasses are improved over the overall correlation with mean atomic weight (Fig. 1B). Error bars are 2σ uncertainty in the mean.

There are significant correlations between IMF and the chemical compositions of glasses. This is illustrated in Fig. 4, where IMF has been plotted against $(X_{Na}/(X_{Na} + X_K))$ for glasses having compositions that correspond to the alkali-feldspar solid solution, and against mole fraction of (Fe + Mn) and Ca for glasses rich in those elements (compare with the data for minerals in Fig. 3). These data suggest that instrumental mass fractionations of oxygen isotopes are also influenced by chemical abundances in glasses. Chemical correlatives with IMF in glasses must differ in detail from those for minerals, however, as is evident by comparing instrumental mass fractionations for minerals and glasses of the same chemical composition (Table 3). Only the quartz-silica glass fractionation is within 1σ of 0‰, and albite, orthoclase and jadeite show a mineral–glass fractionation that is significant at better than the 3σ level. This mineral–glass difference appears on first inspection to be random, i.e. both positive and negative differences are seen, and they are evenly spread over a 5‰ range.

A potentially meaningful correlation between sample chemistry and IMF in glasses can be seen by making the distinction between the atomic masses of network-forming and network-modifying cations. For each pair of mineral and corresponding glass having the same chemical composition, we have calculated the average atomic mass of network-modifying cations (i.e. Ca, Na, K, Fe, Mg, Mn, and non-tetrahedral Al), and taken the difference between this value and the average mass of network-forming cations (i.e. tetrahedrally coordinated Si and Al). This difference has been plotted against the difference in IMF for minerals and glasses of a given composition in Fig. 5. Silica glass contains no network-modifying cations, and has been plotted at 0. The well defined positive correlation demonstrates that compositions with network-modifying cations lighter than Si are less fractionated than their mineral equivalent, and vice versa. In the context of the first-order observation that materials rich in high-

Table 3
Differences in IMF for minerals and glasses

Composition	IMF_{Glass}	$IMF_{Mineral}$	$IMF_{Mineral} - IMF_{Glass}$
SiO_2	-72.94 ± 0.17	-72.83 ± 0.50	0.11 ± 0.53
Albite	-67.34 ± 0.55	-69.64 ± 0.30	-2.31 ± 0.63
Orthoclase	-70.24 ± 0.34	-67.66 ± 0.24	2.58 ± 0.42
Jadeite	-69.71 ± 0.29	-71.79 ± 0.22	-2.08 ± 0.36
UWG-2 Garnet	-61.12 ± 0.37	-60.39 ± 0.31	0.73 ± 0.48

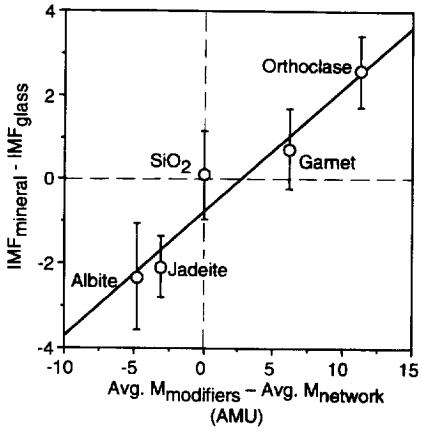

Fig. 5. Differences in IMF between minerals and glasses of the same chemical composition show a correlation with the contrast in mass (M) between network-forming (Si, Al^{IV}) and network modifying (Na, K, Mg, Fe, Ca, Mn, Al^{VI}) cations. Quartz contains no network-modifying cations and has been plotted with value of 0 in the X-axis. This correlation may reflect preferential loss of some elements from the surfaces of glasses during sputtering (e.g. Na, K). Error bars are 2σ uncertainty of the mean.

mass cations are relatively less fractionated (Fig. 1), the fraction of the formula weight found in the network-modifying cations is under-represented.

4.3. Sputter rate

The observed correlations between IMF and various measures of sample chemistry and/or crystallinity described above could be used as the basis of empirical corrections of matrix effects. However, these correlations are of limited use for understanding the causes of these effects because there is little theoretical justification for the choice of variables. We observe that certain chemical parameters 'work' as correlatives with the instrumental mass fractionation among a subset of samples; many equally reasonable variables do not.

In order to further constrain the causes of matrix effects, we have conducted a series of sputtering experiments. A ~7.5 nA, 20 μm diameter, Cs^+ primary beam with a 14.15 keV impact energy and an angle of incidence of 25° (from normal) was rastered over an area of 150 × 150 μm for 45 min each on crystalline Amelia albite (of unknown orientation) and seven silicate glasses. Similar experiments were performed on Amelia albite and zircon on a different date (Table 4). The depths of resulting pits were measured with a Tencor™ alpha step 200 surface profiler, with a reproducibility for multiple

Table 4
sputtering experiments

	Depth of raster pits (nm)	Primary beam current (nA)	IMF (‰) [a]	Sputtering yield [b]	C_{Cs} (%) [c]
Session 1 (150 × 150 μm)					
Albite glass	215.0	7.68	−67.34 ± 0.55	2.65	27.4
Na–Melilite glass	240.0	7.56	−68.58 ± 0.64	3.19	23.9
Jadeite glass	267.5	7.56	−69.71 ± 0.29	3.42	22.6
519-4-1 basalt	192.5	7.51	−64.94 ± 0.11	2.55	28.2
Albite	262.5	7.42	−69.64 ± 0.30	3.68	21.3
HSQ glass	325.0	7.32	−72.94 ± 0.17	3.92	20.3
MK1-8 basalt	175.0	7.42	−63.44 ± 0.32	2.44	29.1
Orthoclase glass	267.5	7.42	−70.24 ± 0.34	3.23	23.6
Zircon [d]			−36.30 ± 0.34	2.90	25.6
Session 2 (125 × 125 μm)					
Albite	389.2	7.0			
Kim-2 zircon	261.0	7.0			

All measured after 45 min sputtering by 14.15 keV Cs^+, 25° angle of incidence, rastered over an area of 150 × 150 μm (session 1) or 125 × 125 μm (session 2). Pit depths are reproducable to ±5 nm.

[a] Average for multiple determinations.

[b] Sample atoms removed per incident Cs atom.

[c] Concentration of implanted Cs (C_{Cs}) = $1/(1 + Y)$ at steady state, where Y is the sputtering yield.

[d] Normalized to constant sputter rate for albite in sessions 1 and 2.

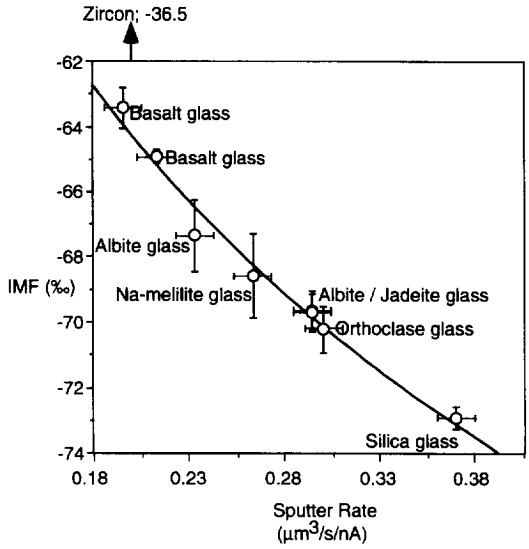

Fig. 6. Instrumental mass fractionations (IMF) plotted vs. sputter rate, as measured by timed rastering experiments made independently of the analyses (Table 4). Data for albite and glasses are plotted; the arrow indicates the location along the horizontal axis of the point for zircon (IMF −36.5‰). Error bars in IMF are 2σ uncertainty in the mean. Errors in sputter rate are based on 2 s.d. reproducibilities in the measurement of raster pit depths. Multiple measurements of the same material have been averaged.

measurements of a single pit of ±5 nm. Measured primary beam currents varied by 5% (total range). The second set of experiments on albite and Kim-2 zircon yielded a sputter rate for albite that differed by 10% from that for the first set, likely due to systematic errors in the estimated width and shape of any given set of raster pits. The sputter rate for zircon has been adjusted by this amount for comparison with the other glasses.

The results of sputter experiments show instrumental mass fractionation to be very strongly correlated with sputter rate among all seven glasses plus albite, including one of the glass–mineral pairs (albite–albite glass) showing a significant difference in fractionation (Fig. 6). Zircon is an exception to this correlation, having a smaller absolute value of IMF than observed in basaltic glass with a similar sputter rate. We note that zircon is the only material on which these experiments were performed that is rich in a very high-mass cation (17 mole% Zr = 91.2 AMU). The correlation among quartzo-feldspathic glasses and basalts displays a gentle curvature, and is well fit by a logarithmic curve ($r > 0.99$; data fit with a mean deviation of ±0.26‰). The simple relation between instrumental mass fractionation and sputter rate among chemically similar materials has important implications for the possible causes of matrix effects in the SIMS analysis of oxygen (discussed below).

Given that our sputtering experiments and most of our analyses used fixed times and primary beam currents, there is also a correlation between IMF and pit depth among the quartzo-feldspathic and basaltic materials. It is therefore relevant to question whether or not a steady state was achieved during the course of individual analyses. We monitored and routinely observed there to be no consistent trend in the measured $^{18}O/^{16}O$ ratio over the course of analyses. The lack of measurable drift is supported by the comparison between the typical analyses and those made with long count times (approximately 3× normal). These analyses showed no degradation of the ratio of expected vs. actual internal precision, and yielded the identical instrumental mass fractionation as found for shorter analyses of the same material in the same analytical session (Table 2). This would not be possible if the instrumental mass fractionation were significantly affected by transient effects. The bottoms of several of the raster pits were analyzed by electron microprobe. They were indistinguishable from the bulk in all elements analyzed, and thus sputtering does not appear to have induced micron-scale chemical changes in the samples.

4.4. Crystallographic orientation

A possible control of instrumental mass fractionation that has not been explicitly tested for oxygen isotopes before is differences in crystallographic orientations of the same mineral. A dependence of the D/H instrumental mass fractionation on orientation has been observed in muscovite (Deloule et al., 1991) suggesting this as a possibility, although previous analyses of oxygen isotope ratios in randomly oriented grain mounts suggest that this is not a significant factor for some minerals (e.g. diopside, zircon, garnet, olivine; Valley et al., 1997b; unpublished data; this study). However, if orientation were to effect IMF, this would potentially be among the

most troublesome of all possible confounding variables in the study of geologic specimens in thin section. We have assessed this possibility in detail for quartz, which has a significant structural anisotropy and might be expected to be representative of silicate minerals in this regard. Two cubes were sawn from an oriented quartz crystal and mounted in epoxy such that one surface exposed the [001] plane (i.e. with the *c*-crystallographic axis oriented perpendicular to the sample surface) and the other exposed a surface orthogonal to the [001] plane (i.e. with the *c*-axis parallel to the sample surface). These faces were each analyzed repeatedly for $^{18}O/^{16}O$ ratio, following the techniques described above. Finally, a sputter experiment as described above was also conducted on each sample. The results (block 13; Table 2) show the instrumental mass fractionation and sputter rate to be indistinguishable for these two crystallographic orientations.

5. Discussion

The results of this study provide new insights into isotopic fractionations in complex samples. Our observations can be summarized as follows.

(1) IMF for oxygen isotopes, measured under the same experimental conditions, varies by up to 36.6‰ among different silicate and phosphate minerals and glasses (after correction for day-to-day variations on any one reference phase).

(2) Correlations are observed between IMF and various measures of sample composition (e.g. mean atomic mass for sub-sets of minerals, mole fraction of solid solution components, elemental abundances in minerals and glasses).

(3) Within the context of such correlations, network-modifying cations appear to be under-represented as a fraction of the mean atomic mass in glasses, in comparison to minerals of the same composition.

(4) IMF is highly correlated with sputter rate among silicate glasses and albite.

(5) IMF and sputter rate in quartz are independent of crystallographic orientation.

The correlatives we have observed with IMF could be used for empirical standardization of ion microprobe analyses of oxygen isotope ratios, several of which will be discussed at the end of this paper. However, the ultimate goal of this and related studies is to develop a robust, general method of standardization, analogous to the correction schemes developed for the electron microprobe. Doing so will require that the physical processes responsible for isotopic matrix effects be understood and that the sample properties truly controlling them be identified. In the following section we will describe two mechanisms that we hypothesize may contribute to matrix effects in oxygen isotope analyses and quantitatively test these hypotheses with our data where possible. These are: (1) transfer of kinetic energy to oxygen atoms during collisions in the zone of sputtering; (2) variations in the ionization probability of oxygen.

Model (1) is quantitatively predictive of differences in IMF among a significant subset of the materials we have studied, while model (2) appears to be a plausible contributing factor but is not yet quantitatively testable.

5.1. Kinetic effects (model 1)

5.1.1. Background

The basis of the proposed kinetic mechanism is that the isotopes of oxygen will be fractionated from one another during sputtering due to differences in the efficiency with which kinetic energy is transferred to each of them by the collisions by which they are ejected. We will show below that materials with relatively high mass constituent atoms are expected to transfer kinetic energy more efficiently to ^{18}O than to ^{16}O, and that this should lead to the over-representation of ^{18}O within the population of secondary ions sampled relative to an analysis free of this phenomenon. This is expected due to two effects: (1) a higher proportion of the population of ^{18}O atoms will be sampled at high-energy offsets due to the broadening of its energy distribution relative to that of ^{16}O (e.g. see Thompson, 1968 for a general treatment on energy distributions of sputtered atoms); and (2) over a finite range of high-energy offsets (e.g. the 324–376 eV population analyzed in this study), the average energies of all ^{18}O atoms falling within that range will be higher than that of all ^{16}O atoms, again due to the broadening of the ^{18}O energy spectrum at high energies. Ionization probability in-

creases with increasing initial kinetic energy of the sputtered atoms (i.e. prior to acceleration by the extraction voltage) by common models of electron loss/capture during sputtering (Yu and Lang, 1986) or bond breaking (Gerhard and Plog, 1987) and thus the ratio of ionization probabilities (P) for ^{18}O and ^{16}O (P_{18}/P_{16}) will be higher than would be expected for a population of oxygen atoms all having exactly equal initial kinetic energies. We will begin the discussion of this model with a general discussion of secondary ion production.

The collision of a primary ion with a target surface includes a chain of primary collisions (primary ion-sample atom) and a much larger set of secondary collisions between sample atoms, which may be quite diverse in complex materials (Williams, 1979). Secondary oxygen ions may result from many of these various chains of collisions, but simple consideration of the collision dynamics and the details of our analysis suggests that we sample only a select portion that discards the products of all but a small sub-set of the possible chains of collisions. Molecular dynamics calculations for sputtering of SiO_2 by Cs indicates that a significant yield of 300–400 eV oxygen atoms will be emitted from the surface due to simple, one-step collisions with the primary ion having an angle of incidence approximately equal to that in our experiments (J. Harman and T. Tombrello, pers. commun.). However, these are emitted at an angle of $< 30°$ relative to the sample surface, and secondary oxygen ions of the energy analyzed must be emitted with angles of $> 75°$ to pass the aperture in the extraction cover plate on the Cameca ims-4f. Thus, our analyzed population must result from the more complex chain of collisions within the sample itself. Only a small subset of atoms ejected by this means have a large kinetic energy and those atoms that are ejected are likely to be the result of short collision chains involving atoms near the sample surface (Williams, 1979), which may include original (pre-sputtering) sample components or an implanted Cs atom. The concentration of implanted Cs will be shown to be a particularly important variable in this model. It has been estimated, where possible, by the relationship:

$$C_{Cs} = 1/(\text{sputter yield} + 1) \quad (3)$$

where the sputtering yield is equal to the number of sample atoms sputtered divided by the number of Cs ions by which the sample has been bombarded. Eq. (3) is a direct consequence of the establishment of a steady state during sputtering, and describes the average concentration of Cs in the near-surface region from which secondary atoms are sputtered.

Several physical mechanisms may lead to a small proportion (1 in 10^1–10^6) of ejected atoms becoming ionized (Yu and Lang, 1986). Following collision, a sample atom has a kinetic energy imparted to it which may be tens to hundreds of times the energy of chemical bonds ($\sim$ 1–5 eV; Dean, 1985). The valence electrons associated with this atom become elevated to an excited state, and relaxation of these electrons to a lower-energy state may result in that atom gaining or losing electrons taken from or given to the population of conduction band electrons (in metals) or chemical bonds (for ionic or covalently bonded solids) that the atom shared prior to collision (e.g. Shroeer et al., 1973; Slodzian et al., 1980; Yu and Lang, 1986). Several variables influencing one or both of these mechanisms are known to cause isotopic fractionations (e.g. the relative masses of the analyzed isotopes, the energy of detected secondary ions, the angle between emitted secondary ions and the sample surface, and first ionization energies of secondary atoms), and it has been observed that secondary ions with high initial kinetic energies sputtered from elementally pure targets exhibit IMF's that are negative and tens of permil in magnitude (Shimizu and Hart, 1982). These fractionations are reasonably attributed to differences between the ionization probability for different isotopes, approximately following the law: $\alpha_{SIMS} = M_{light}/M_{heavy}$ (expected to yield a value of $-111‰$ for oxygen). Those factors which might be expected to lead to differences between different materials in IMF for a given element include lattice bond energies (for the bond breaking model), the binding energy of the surface, and differences in the kinetic energy between isotopes. Consideration of data for bond and surface energies suggests that they are unlikely to explain our observations. Both energetic barriers vary over a limited range of values (1–5 eV) that are small compared to the energies of ions detected in this study (324–376 eV), and that are not simple functions of atomic mass (making it unlikely that

they could lead to correlations such as those in Figs. 1–6). This suggests that the isotopic matrix effect can be more readily explained by considering kinetic factors. This simplifying assumption is a result of our analyses including only very high-energy secondary ions. Matrix effects for low-energy secondary oxygen ions may be expected to be dependent upon bond-energy and other energetic barriers, as has been suggested for D/H ratio measurements in amphiboles and micas (Deloule et al., 1991).

5.1.2. Derivation of the kinetic effect

It is both predicted by collision theory and observed by experiment that the secondary ion energy spectrum has a relatively simple shape at high energy, decaying approximately proportionally to E^{-2}, and that the abundance of secondary ions of a given energy is proportional to the maximum energy those ions can have by collision with a primary ion (Thompson, 1968; Shroeer et al., 1973; Engstrom et al., 1987; Gerhard and Plog, 1987):

$$N_E \propto \gamma \cdot E_p \tag{4}$$

where N_E is the secondary ion abundance at a given energy, γ is the ratio of the maximum kinetic energy of a secondary atom to the energy of the primary atom and is a simple function of their relative masses (e.g., Eq. (6), below), and E_p is the energy of the primary ion. At high energy where these approximations apply, the relative yield of secondary ^{18}O and ^{16}O ions will therefore be proportional to the maximum energy that either ion can acquire from the collisions that ejected it from the sample:

$$N(^{18}O)/N(^{16}O) \propto \gamma_{18}/\gamma_{16} \tag{5}$$

We will assume that the transfer of kinetic energy between atoms during the chain of primary and secondary collisions is purely elastic and, following the reasoning above, will simplify the large array of possible collision paths to consider only one in which energy is transferred from a primary ion to a matrix atom, which then strikes and ejects an oxygen atom. We will neglect angular terms as a simplification. The in-elasticity of collisions may be an important neglected variable in these calculations, but the latter two assumptions should not influence the sensitivity of the calculated kinetic effect to mass unless the numbers and angles of individual collisions leading to ^{18}O sputtering were systematically different from those leading to ^{16}O sputtering. Conservation of momentum and energy dictate that the efficiency is:

$$\gamma = \left((4 \cdot M_p \cdot M_i)/(M_p + M_i)^2\right) \cdot \left((4 \cdot M_i \cdot M_s)/(M_i + M_s)^2\right) \tag{6}$$

where subscript p denotes the primary ion, i the intermediate matrix atom, and s the secondary ion, E is the kinetic energy, and M the mass. It follows that the kinetic matrix effect for sputtering of ^{18}O and ^{16}O is predicted to be:

$$\gamma_{18}/\gamma_{16} = \left((4 \cdot M_i \cdot M_{18})/(M_i + M_{18})^2\right) / \left((4 \cdot M_i \cdot M_{16})/(M_i + M_{16})^2\right) \tag{7}$$

Derivations of isotopic or chemical fractionations which have also considered the energetic barriers to sputtering and ionizations yield very similar results. Bond-breaking models predict the relationship:

$$N \propto U/E.\gamma^n \tag{8}$$

where U is the bond energy, E the initial secondary ion energy and n a fitted parameter (e.g., Gerhard and Plog, 1987). Similarly, 'tunneling' models predict:

$$N \propto \left(E_{avg}\right)^n \tag{9}$$

where E_{avg} is the average energy of secondary ions and is a function of the surface bonding energy and n is again a fitted parameter (Shroeer et al., 1973; Shimizu and Hart, 1982). Both Eqs. (8) and (9) reduce to a functional form very similar to that derived here for the case of the isotope ratio N_{heavy}/N_{light}, and in both instances there is only a weak relationship between N_{heavy}/N_{light} and surface or bond energies for secondary ions in the 10^2–10^3 eV range. The ratio γ_{18}/γ_{16} is equal to the ratio of 'energy transfer factors' of Gerhard and Plog (1987) for the two isotopes. Fitted exponential parameters in similar previous work are interpreted as material specific, and would thus be expected to cancel for the ratio N_{heavy}/N_{light} (i.e. only if such parameters were specific to an isotopic mass in a given material should they exist in Eq. (7)). Given the absence of any theoretical justification for their use, we will not include a fitted term in calculating the expected relationship between target mass and matrix effects.

5.1.3. General expectations of kinetic factors

We have calculated values of energy transfer efficiencies (γ_i), isotopic matrix effects (γ_{18}/γ_{16}) and relative sputter rates for a range of atomic masses of the intermediary atom (M_i) between 1 and 133 AMU. These calculations assume an incident atom of $^{133}Cs^+$ striking a matrix atom of mass M_i, followed by a collision between the matrix atom and either ^{18}O or ^{16}O. The relationships among M_i, energy transfer efficiency (γ) and the isotopic 'kinetic effect' predicted by Eq. (7) (in units of permil) are plotted in Fig. 7. Absolute values of γ_i are highly sensitive to the details of the number and angle of collisions, although the sensitivity of variations in γ_i to mass, and therefore γ_{18}/γ_{16} ratios, should not be sensitive unless the collision sequences leading to secondary ion production differed consistently between ^{16}O and ^{18}O. The results show γ_i to be a very sensitive positive function of M_i between M_i-values of 1 and 40, after which γ_i decreases gently. One consequence of this relation is that in compositionally heterogeneous targets, collisions between O and relatively high mass atoms will be over-represented as a fraction of all sputtered O (at any specified high initial kinetic energy). This factor is expected to result in non-linearities in the dependence of IMF on stoichiometry in some instances. The kinetic contribution to IMF is predicted to increase continuously with mass, from very low values for light elements (e.g. −105‰ for H) up to +91‰ for Cs. The dependence upon mass is significantly greater below $M_i = 50$ than at high M_i. Variations in γ_{18}/γ_{16} over the range of masses for the constituent atoms in most if the materials studied is 66‰ ($16 \leq M_i \leq 55$; this range increases to 91 and 99‰ if Zr and implanted Cs, respectively, are included). Thus this mechanism appears capable of producing variations in IMF of 10's of ‰, which correlate with the mass of target components and, due to the influence of implanted Cs, with sputter rate. These are true for our observations, suggesting that this mechanism is a possible cause of some of the variations in IMF that we have seen.

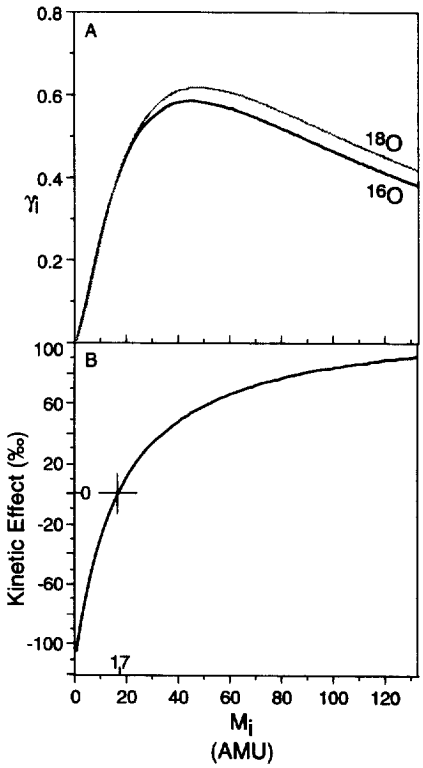

Fig. 7. Predicted relationship between instrumental mass fractionation for oxygen isotopes and sample atomic mass, based on kinetic model described in the text. (A) The efficiency for transfer of kinetic energy from primary to secondary ion (γ_i; see Eq. (6)) as a function of the mass of the intermediate atom, M_i, in a three-atom collision sequence. Intermediate atoms with mass greater than 17 AMU transfer energy more efficiently to ^{18}O than ^{16}O and vice versa. This difference in maximum kinetic energy for different isotopes of oxygen translates into differences in the number of secondary ions at a given (high) secondary energy. (B) The resulting fractionations (≡ kinetic effect) in units of ‰ (where 0.0 is the isotopic ratio in the absence of this kinetic matrix effect, and occurs at $M_i = 17$).

5.1.4. Sensitivity of kinetic factors to compositional variables in silicates

The preceding generalities indicate that the contribution of any given element to the IMF observed in a multi-component target may be a complex function of its mass and the mass of other components. We have calculated the expected sensitivity of IMF to the addition of several major oxide components and implanted Cs to SiO_2 (Fig. 8) as a means of exploring expected kinetic effects among silicates with variable sputter rates. These calculations were made using the following equation to weight values of γ_i for the abundance of each element:

$$\gamma_{18}/\gamma_{16} = \Sigma(X_i \cdot \gamma_{18})/\Sigma(X_i \cdot \gamma_{16}) \quad (10)$$

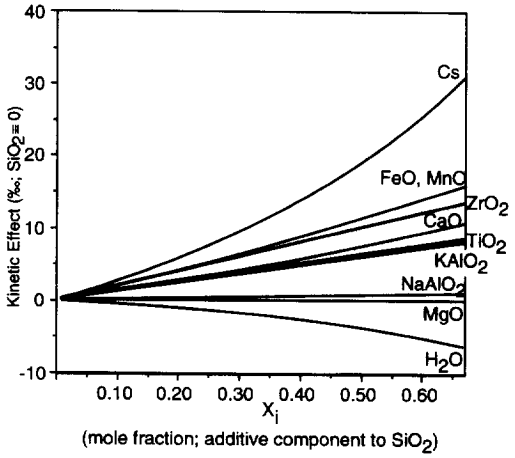

Fig. 8. Predicted sensitivity of kinetic effects to major compositional variables in the zone of sputtering, calculated as additive components to SiO_2. The effect of Cs implantation is expected to be highly significant given the concentrations of 10's of % implied by our sputter rate determinations and Eq. (3).

were X_i is the mole fraction of elemental component i in the zone of sputtering, and γ_i values are derived from Eq. (6) with that component as M_i. We emphasize prior to discussing the results of these calculations that they are only predictive of the sensitivity of IMF to the composition of the zone of sputtering, which will differ significantly from the bulk, principally due to implanted Cs but also possibly due to preferential sputtering, Gibbsian segregation and/or other sputtering-induced modifications. A worked example of the following calculations is provided in Appendix A.

It is apparent from Fig. 8 that the most important compositional parameter one must know in quantitatively predicting this effect for most silicates is the concentration of implanted Cs, which is known to vary significantly and at substantial levels in the materials in Fig. 6 (20–30%, based on Eq. (3) and estimated densities). ZrO_2, FeO and MnO (as well as $FeO_{1.5}$, not shown) are predicted to be second only to implanted Cs as compositional controls of IMF in silicates. CaO, $KAlO_2$ and TiO_2 exert an intermediate influence relative to other common mineral components, while MgO and $NaAlO_2$ are expected to have no substantial influence as additive components to SiO_2. H_2O is predicted to lead to moderate decreases in IMF relative to pure SiO_2, but this effect should be minimal over the common range of water contents in minerals and most glasses. The predictions of variations in IMF among compositions equal to the bulk minerals and free of implanted Cs are not expected to be accurate. We note, however, that most of the first order-expectations are met; i.e. compare the relative order and approximate magnitude of the observed variations in IMF with various elemental concentrations in Fig. 3 and the predicted sensitivity in Fig. 8.

5.1.5. *Predicted relationship between sputter rate and IMF*

Given the strong predicted kinetic effect of implanted Cs and the concentrations of 20–30% implied by sputter rates measured in some of our samples (calculable using Eq. (3) and values for sample density), a prediction of this model is that sputter rate should be well correlated with IMF among materials whose pre-sputtering components are similar. We have quantified this prediction through two calculations, one predicting the dependence of IMF on sputter rate in a material of fixed composition (i.e. other than variable implanted Cs content), and the other predicting the magnitude of the kinetic effect for the nine materials in which sputter rate and major element compositions prior to sputtering are known.

Fig. 9A presents the calculated variation of the kinetic effect with sputter rate, based only upon the effect of variations in the concentration of Cs. The kinetic effect was calculated using Eq. (10), assuming that the site of sputtering is stoichiometric SiO_2 plus the amount of Cs calculated for a given sputtering rate (using a density of 2.65 g/cm^3 and Eq. (3)). The extent of the predicted effect agrees quite favorably with the observations for silicate glasses and albite. This result indicates that the kinetic consequences of Cs implantation into the zone of sputtering alone can account for much of the variability in IMF observed in materials with broadly similar chemistry.

Finally, we have calculated the predicted kinetic effect on IMF for the materials on which sputtering experiments were performed, using the implanted Cs concentrations estimated from Eq. (3) and assuming that the remainder of the zone of sputtering was

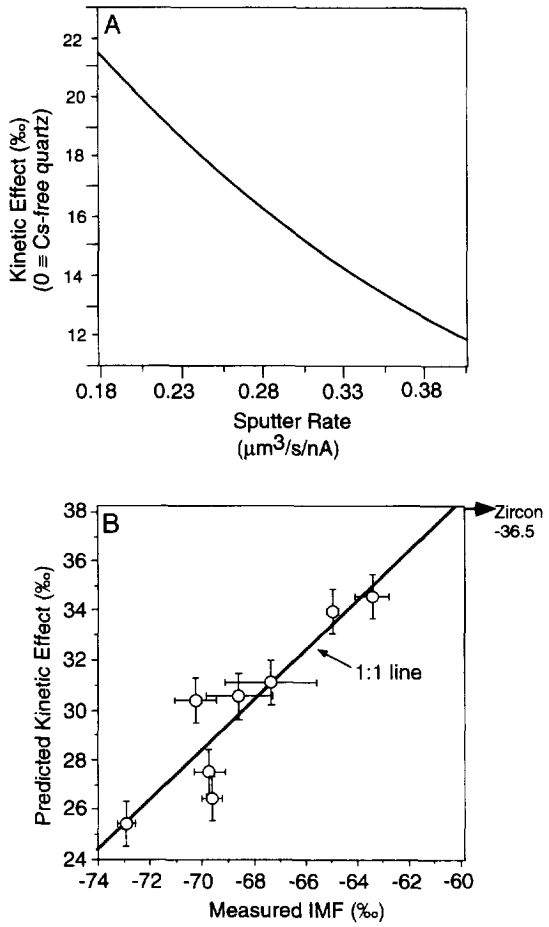

Fig. 9. Quantitative predictions of the kinetic model. (A) The kinetic effect of Cs implantation alone (i.e. other compositional variables held constant) is predicted to produce a gently curved, negative correlation between IMF and sputter rate. The curve was calculated for SiO_2 with a density of 2.65 g/cm^3. The result is plotted at the same *X*- and *Y*-axis scales as Fig. 6, and shows a very similar dependence as seen in the data for albite and silicate glasses. (B) Predicted kinetic effects in the nine materials for which sputtering rates were determined (Table 4), including the inferred concentration of implanted Cs from Eq. (3), and assuming that the remainder of the zone of sputtering has a composition equal to the bulk prior to sputtering. This assumption is likely to be poor if Fe, K and Ca are enriched or diminished by a factor 2 or more in the phases rich in each of those components, and for zircon if Zr is enriched or depleted by more than 20%. The 1:1 correspondence among albite and the silicate glasses indicates that kinetic effects can account for the variations in IMF observed in these materials. The deviation from the 1:1 line for zircon (location on vertical axis indicated with arrow) indicates either Zr enrichment in the sample surface during sputtering or the action of some other mechanism for producing matrix effects.

equal in composition to the bulk material prior to sputtering. This latter assumption is almost certainly incorrect in detail, but an alternative cannot be justified without data on surface chemistry and it is likely not to introduce significant uncertainty for albite and the silicate glasses because of the expected sensitivity of IMF to sample components (Fig. 8). In order for errors of several permil to be introduced by this approximation, the contents of Fe, Ca (in basalts) and K (in orthoclase) must be enriched or depleted by more than a factor of 2. Variations among the relative abundances of Si, Al, Na and Mg are not predicted to have significant effects. An exception to this is zircon, which is rich in a component that is very high in mass and is predicted to have a large effect on IMF by this mechanism. If sputtering produces changes of more than 20% in the ratios Zr/Si or Zr/O in the surface of zircon, then the predictions of this calculation will be seriously in error. Other uncertainties in the calculations are: ± 10 nm in pit depth ($2\times$ our average reproducibility of measurements), which propagates to an uncertainty of ± 0.6‰ in the calculated index, and errors in glass and mineral densities, which we estimate at ± 0.1 g/cm^3, leading to a propagated uncertainty of ± 0.7‰. Therefore, other than the systematic errors inherent to our assumption of stoichiometry for this calculation, we estimate errors in predicted kinetic effects to be ± 0.9‰.

The resulting predictions are compared to the data in Fig. 9b. There is a 1:1 correlation over a 10‰ range for albite and the silicate glasses. This result confirms the conclusion reached by comparing Figs. 6 and 9a; i.e. differences in kinetic effect (principally due to variations in the amount of implanted Cs) accurately predict the direction and magnitude of differences in IMF among materials that are broadly related in their chemistry. The relative difference in IMF between zircon and these materials is not correctly predicted, however. This may reflect large changes in the chemical composition of the surface, such that more Zr is present than in stoichiometric zircon, or may indicate an additional factor or mechanism that influences IMF but is not part of the kinetic model. Resolution of this question will require further work, particularly studies of surface chemistries of sputtered silicates and analysis of more materials rich in very high mass cations.

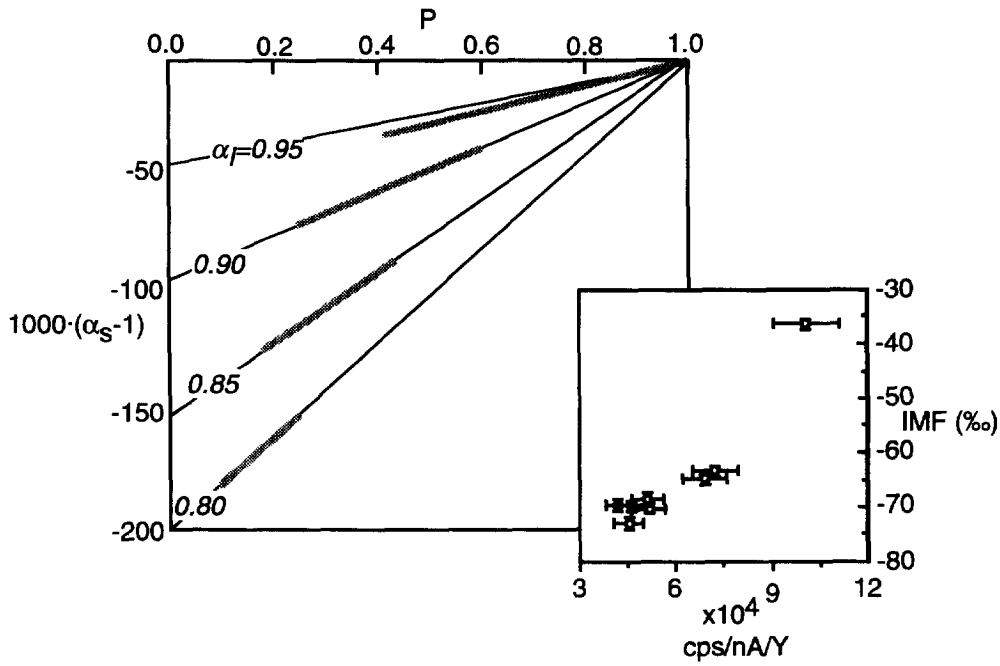

Fig. 10. Dependence of the isotopic difference between ionized oxygen and all sputtered oxygen of a given energy (α_S, in units of ‰) on the probability of ionization (P), as calculated with Eq. (14). Light lines indicate results for a variety of values of α_I (the fractionation between ionized and non-ionized atoms). The lever rule requires that as P approaches 1, the ionized atoms must approach the isotopic composition of all sputtered oxygen having the secondary energies analyzed, regardless of α_I. Heavy line segments indicate ranges of P for a given α_I that could satisfy the correlation seen in our data between IMF and the value: counts per second/nA primary beam current/Y, where Y is the number of atoms sputtered per incident Cs ion (inset). This index should be proportional to P under constant instrumental conditions. Error bars for IMF are 2σ uncertainty in the mean. Error bars for Cps/nA/Y are 10% of the calculated value, a conservative estimate of the range of drift observed in the primary beam current and secondary ion count rate over the course of analyses.

5.2. Ionization probability

In the following paragraphs we briefly examine a second mechanism, by which matrix effects are caused by variations in the ionization efficiency of sputtered atoms, independent of the isotopic fractionation that accompanies ionization. This mechanism may be suggested by the data in this study, and is more strongly indicated by preliminary analysis of variations in IMF among carbonate minerals (Eiler et al., 1997).

Variations in ionization efficiency have the potential of producing large variations in IMF through the simple operation of the lever rule: mass balance requires that as the probability of ionizing sputtered atoms (P) approaches 1, the secondary ion population must approach the isotopic composition of the entire population of atoms sputtered within the range of initial kinetic energies analyzed, regardless of the mass fractionation caused by ionization. This can be expressed in the following equations. We define: $R = {}^{18}O/{}^{16}O$, and subscripts I, NI and S respectively denote the ionized secondary atoms, non-ionized secondary atoms and the weighted sum of all secondary atoms having the specified initial kinetic energies.

$$\alpha_I \equiv R_I/R_{NI} \tag{11}$$

$$\alpha_S \equiv R_I/R_S \tag{12}$$

$$P \cdot R_I + (1-P) \cdot R_{NI} = R_S \tag{13}$$

It follows:

$$\alpha_S = 1/[P + (1-P) \cdot (1/\alpha_I)] \tag{14}$$

The expected correlation between α_S and P based on Eq. (14) is plotted in Fig. 10 for values of α_I between 1.0 and 0.8 (among the more extreme in-

ferred for any element and more extreme than any reported for total instrumental mass fractionation for oxygen isotopes). Note that R_S need not equal the isotope ratio of the bulk sample for the particular range of secondary ion energies analyzed and therefore α_S is expected by this model to be proportional to but not equal to α_{SIMS}.

This mechanism could produce a correlation such as that seen among albite and the silicate glasses in Fig. 6 due to the dependence of ionization efficiency upon the concentration of implanted Cs. It is well established that the surface concentration of implanted Cs exponentially increases the probability of ionization for negative ions by lowering of the work function (the energy required to extract an e^- from a surface; see review by Yu and Lang, 1986). Testing this model requires estimates of relative differences in P among the materials analyzed. We have done so using the approximation that $P \propto$ (counts per second)/(primary beam current/Y); a relation that assumes there are no systematic differences in transmission or detection efficiency between the materials studied (inset to Fig. 10). The eight materials demonstrating a good correlation between IMF and sputter rate in Fig. 6 had only a 10% range in secondary ion count rates under constant instrumental conditions, despite a range of a factor of 1.6 in their sputtering yield. This suggests that P varied by approximately a factor of 1.6 among these materials. If so, the ratio of ionized to non-ionized sputtered atoms was positively correlated with IMF, and this simple lever-rule effect may be significant. A 10‰ range in α_S over a factor of 1.6 range in P will only occur if values of P are greater than 0.1 for any $\alpha_I > 0.8$ (Fig. 10). Count rates for zircon were significantly higher at a given set of instrumental conditions than observed in albite and the silicate glasses, extending the range in IMF to 36.5‰ over a factor of 2.4 range in cps/nA/Y. If this is the result of a lever-rule effect, the lowest value of P is constrained to be ≥ 0.2, and $\alpha_I \leq 0.94$ (and if α_S is close to the observed α_{SIMS}, $0.24 \geq P \geq 0.56$ and $\alpha_I = 0.903$ for the materials studied).

The presence of a correlation between (cps/nA/Y) and IMF among our samples indicates that this mechanism may contribute to the matrix effects we have observed. However, this correlation contains substantial scatter and is not compelling in detail. The 'lever rule' and kinetic mechanisms are not mutually exclusive, and it is possible that the partial success of both with subsets of the data (i.e. the kinetic effect for silicate glasses, the 'lever rule' for zircon) indicate that both take place. The values for P suggested by application of this model to our data (> 0.1) are exceptionally high relative to common estimates, but may be possible for the very high initial kinetic energies of the ions we have analyzed. More quantitative tests of this hypothesis based on our existing data are not possible given that P, α_I and the dependence of P upon C_{Cs} in the materials studied is not known.

All of the above discussion has been aimed at finding correlations with and causes of variations among universally large, negative values of IMF. The trends to our data in Fig. 9b and Fig. 10 suggest that values of IMF are likely to be approximately -100‰ in the absence of kinetic and/or 'lever rule' effects. This is close to the value of -111‰ expected for a fractionation during ionization following the M_{light}/M_{heavy} law noted for high-energy secondary ions emitted from pure metals (Shimizu and Hart, 1982), and thus suggests that this fractionation during ionization may be the cause of large negative fractionations among all materials in this study.

6. Summary and conclusions

Instrumental mass fractionations in the analysis of oxygen isotopes are large under the analytical conditions of this study (-74.7 to -30.3‰), but they routinely yield point-to-point precisions expected from counting statistics (± 1.0–0.5‰, 1 s.d.) within a given analytical session. A large portion of the instrumental mass fractionation is related to sample properties, with a general tendency of materials having a high atomic mass to yield less fractionated isotope ratios. Chemical correlatives with IMF are shared among different mineral groups and are in some cases very robust (e.g. Fe + Mn; Fig. 3). We find no evidence for structural effects on the instrumental mass fractionation in minerals. Differences in IMF are observed between minerals and glasses of the same composition (Fig. 5), and we speculate that

they reflect compositional modifications in the zone of sputtering in glasses, particularly loss of alkali elements in alkaline glasses. A kinetic model for matrix effects accurately predicts the strong correlation between IMF and sputter rate and the relative order and extent of observed instrumental mass fractionations in a set of similar silicates. The data may also be consistent with a second model based upon the application of the 'lever rule' to the populations of ionized and non-ionized sputtered atoms, although this latter model is less easily tested quantitatively and is therefore more speculative.

6.1. Standardization of oxygen isotope analyses

The results of this study suggest several strategies for standardization of SIMS analysis of oxygen isotopes.

Identical chemistry and structure. Analysis of a standard which is chemically and structurally as similar to the unknown as is possible must always be preferred. The results of this and previous similar studies suggest that minor compositional components (~ 1–2%) and crystallographic orientation should not influence IMF. Our data indicate that a comparison of sputtering rates between standard and unknown would also be wise.

Solid solution series. Analysis of minerals that are compositionally zoned or differ from standards in their relative abundance of solid solution end members (or glasses that differ from standards in normative composition) is a more difficult task. The pronounced non-linearity in our data for olivines (Fig. 2) indicates that linear interpolation among end members could introduce very large errors in some cases. However, continuous covariations of IMF with chemical composition is seen among several sub-sets of related minerals and glasses. Interpolation between standards in the dimensions of some chemical variable (e.g. mole fraction Fe or location on a solid solution binary) is therefore suitable if unknowns are closely bracketed by standards. Our data suggest that if interpolations of IMF between standards are modest (2–5‰), a simple interpolation is likely to be within 1‰ of the correct value. This method offers an advantage over standardization with chemically and structurally identical materials. However, this advantage is small because in many cases standards must still be quite close in chemical composition to the unknown.

Elemental content. The abundances of Fe, Mn and Ca in phases rich in those elements were found to be highly correlated with IMF among several mineral groups. The correlation between (Fe + Mn) and IMF in particular fits the data among fifteen structurally diverse samples. This is therefore the simplest and best empirical means of standardizing the analysis of Fe-bearing silicates. Because of the non-linearity of IMF vs. (Fe + Mn) content (Fig. 3), this method should not be used unless the unknown has been bracketed by several standards. It is not suitable for significant extrapolation.

Physical models of the matrix effect. None of the above methods deal directly with the cause of the matrix effect, and we suggest that a preferred method of standardization should ultimately do so. We have proposed two mechanisms for producing matrix effects, both of which are consistent with available data and one of which (the kinetic effect) quantitatively reproduces measured differences in IMF among a significant subset of materials. Further tests of these models and integration of our data with measurements on a more diverse group of samples therefore seems likely to advance physically based models to the point that they are applicable as a general correction scheme. The kinetic effect appears to be a good working model for differences in IMF among some of the most common silicate compositions (i.e. Na–K–Ca–Al silicate minerals and glasses and natural basalt glasses) provided that relative differences in sputter rate are known.

Our study suggests several important goals for future research in the standardization of stable isotope analyses by SIMS. Matrix effects remain essentially unexplored for analyses using low energy offset, and it is possible that they will differ substantially from those observed in this work. In addition, IMF has been observed to be a function of primary beam energy (Schauer et al., 1993), and the interaction of this effect and matrix effects has yet to be explored. Further study of matrix effects under conditions of variable energy offset and variable primary beam energy may reveal optimal conditions for minimizing and/or controlling matrix effects while retaining the level of analytical precision that is now routine.

Acknowledgements

This work was supported by funding from the Department of Energy grant 93ER14389 (JWV), National Science Foundation grants EAR9304372 (JWV) and EAR9303975 (S. Epstein and E. Stolper), and National Energy Research Council grant GR9/01806 (CMG). The invaluable contribution of John Craven to this study in instrument tuning and maintenance, ideas and suggestions, and helpful comments on the manuscript, is gratefully acknowledged. The ion microprobe laboratory is generously supported by NERC. We thank Mike Spicuzza for assistance in the stable isotope laboratory at the University of Wisconsin, and Ed Stolper for his encouragement and financial support of the first author's contribution to this work. The manuscript benefited from thorough and insightful reviews by Ian Hutcheon, Kevin McKeegan and Richard Hervig. We thank Tom Tombrello and John Hartman for their insightful comments on this work, and Serge Nadau, George Rossman and Ian Cartwright for supplying some of the samples for this study.

Appendix A. Worked example of kinetic effect

We present here a worked example of the calculated prediction of the kinetic contribution to IMF. We will use as an example crystalline albite with a density of 2.62 g/cm^3 ($7.82 \cdot 10^{22}$ atoms/cm^3) and sputtering results from Table 4 (i.e., a pit depth of 262.5 nm after sputtering over a 150 μm × 150 μm area for 45 min at 7.42 nA primary beam current). The sputtering yield (Y) equals the number of target atoms sputtered per primary ion that hits the surface:

$$Y = \frac{[(\text{cm}^3\ \text{sputtered}) \cdot (\text{atoms/cm}^3)]}{[(\text{beam current}) \cdot (\text{atoms/nA/s}) \cdot (\text{time})]}$$

$$Y = \frac{\left[\left((1.50 \cdot 10^{-2})^2 \cdot 2.625 \cdot 10^{-5}\right) \cdot (7.82 \cdot 10^{22})\right]}{\left[7.42 \cdot (6.25 \cdot 10^{9}) \cdot (2.7 \cdot 10^{3})\right]} = 3.69$$

The steady state average concentration of Cs (C_{Cs}) in the zone of sputtering is described by Eq. (3):

$$C_{Cs} = 1/(1 + Y) = 0.213$$

The composition in the sample surface is therefore equal to: $(NaAlSi_3O_8)_{0.787}Cs_{0.213}$ (assuming stoichiometric relative abundances of original elements). Values of X_i and γ_i (calculated with Eq. (6)) for each element are:

Element	X_i	γ_{18}	γ_{16}
Na	0.0605	0.4952	0.4865
Al	0.0605	0.5285	0.5242
Si	0.1815	0.5482	0.5325
O	0.4840	0.3821	0.3834
Cs	0.2134	0.4200	0.3834

The predicted kinetic effect is easily calculated using Eq. (10) and the above values, and is 1.0268, or 26.5‰ enriched in ^{18}O relative to the $^{18}O/^{16}O$ that would be observed in the absence of any kinetic effects.

References

Baertschi, P., 1976. Absolute ^{18}O content of standard mean ocean water. Earth Planet. Sci. Lett. 31, 341–344.

Dean, J.A. (Editor), 1985. Lange's Handbook of Chemistry, 13th ed. McGraw Hill, New York.

Deline, V.R., Katz, W., Evans, C.A., Williams, P., 1978. Mechanism of the SIMS matrix effect. Appl. Phys. Lett. 33, 832–835.

Deloule, E., France-Lanord, C., Albarède, F., 1991. D/H analysis of minerals by ion probe. In: H.P. Taylor, Jr., J.R. O'Neil and I.R. Kaplan (Editors), Stable Isotope Geochemistry: A Tribute to Samuel Epstein. Geochem. Soc. Spec. Publ. 3, 53–62.

Eiler, J.M., Valley, J.W., Graham, C.M., Baumgartner, L.P., 1995. Ion microprobe evidence for the mechanisms of stable isotope retrogression in high-grade metamorphic rocks. Contrib. Mineral. Petrol. 118, 365–378.

Eiler, J.M., Valley, J.W., Graham, C.M., 1997. Standardization of SIMS Analysis Of O and C isotope ratios in Carbonates from ALH-84001. 28th Lunar and Planetary Science Conference, in press.

Elsenheimer, D., Valley, J.W., 1992. In situ oxygen isotope analysis of feldspar and quartz by Nd:YAG laser microprobe. Chem. Geol. 101, 21–42.

Engstrom, E.U., Lodding, A., Odelius, H., Sodervall, U., 1987. SIMS yields from glasses; secondary ion energy dependence and mass fractionation. Mikrochim. Acta 1, 387–400.

Farqhar, J., Chacko, T., Frost, R.B., 1993. Strategies for high-temperature oxygen isotope thermometry; a worked example from the Laramie anorthosite complex, Wyoming, USA. Earth Planet. Sci. Lett. 117, 407–422.

Gerhard, W. and Plog, C., 1987. SIMS-matrix effect and model of ion pair production (Part II). In: A. Benninghoven, A.M. Huber and H.W. Werner (Editors), SIMS VI. John Wiley, Chichester, pp. 109–112.

Giletti, B.J., Shimizu, B., 1989. Use of the ion microprobe to measure natural abundances of oxygen isotopes in minerals. In: W.C. Shanks III and R.E. Criss, New Frontiers in Stable Isotope Research. U.S. Geol. Surv. Bull. 1890, 129–136.

Gnaser, H., Hutcheon, I.D., 1987. Velocity dependent isotope fractionation in secondary ion emission. Phys. Rev. B35, 877–879.

Graham, C.M., Valley, J.W., Winter, B.L., 1996. Ion microprobe analysis of $^{18}O/^{16}O$ in authigenic and detrital quartz in the St. Peter Sandstone, Michigan Basin and Wisconsin Arch, USA: contrasting diagenetic histories. Geochim. Cosmochim. Acta 60, 5101–5116.

Hervig, R.L., Williams, P., Thomas, R.M., Schauer, S.N., Steele, I.M., 1992. Microanalysis of oxygen isotopes in insulators by secondary ion mass spectrometry. Int. J. Mass Spectrom. Ion Process. 120, 45–63.

Jamtveit, B., Hervig, R.L., 1994. Constraints on transport and kinetics in hydrothermal systems from zoned garnet crystals. Nature 263, 505–508.

Leshin, L.A., Rubin, A.E., McKeegan, K.D., 1996. Oxygen isotopic compositions of olivine and pyroxene from CI chondrites. Lunar Planet. Sci. 27, 745–746.

Lorin, J.C., Slodzian, R., Dennebouy, R. and Chaintreau, M., 1990. SIMS measurement of oxygen isotope-ratios in meteorites and primitive solar matter. In: A. Benninghoven, C.A. Evans, K.D. McKeegan, H.A. Storms and H.W. Werner (Editors), Secondary Ion Mass Spectrometry, SIMS VII. John Wiley, Chichester, pp. 377–380.

Lyon, I.C., Saxton, J.M., Turner, G., 1994. Isotopic fractionation in secondary ionization mass spectrometry. Rapid Commun. Mass Spectrom. 8, 837–843.

Mattey, D., Macpherson, C.M., 1993. High-precision oxygen isotope analysis of microgram quantities of silicate by laser-fluorination. Chem. Geol. 105, 305–318.

McKeegan, K.D., 1987. Oxygen isotopes in refractory stratospheric dust particles: proof of extraterrestrial origin. Science 237, 1468–1471.

Ricci, M.P., Merritt, D.A., Freeman, K.H., Hayes, J.M., 1994. Acquisition and processing of data for isotope-ratio-monitoring mass spectrometry. Org. Geochem. 21, 561–571.

Riciputi, L.R., Paterson, B.A., 1994. High spatial resolution measurement of O isotope ratios in silicates and carbonates by ion microprobe. Am. Mineral. 79, 1227–1230.

Riciputi, L.R. and Paterson, B.A., 1997. Accurate analysis of $^{18}O/^{16}O$ ratios in chemically-zoned silicates by ion microprobe: an empirical method. Submitted to Geochim. Cosmochim. Acta.

Santos, R.V., Clayton, R.N., 1995. Variations in oxygen and carbon isotopes in carbonatites: a study of Brazilian alkaline complexes. Geochim. Cosmochim. Acta 59, 1339–1352.

Schauer, S.N., Williams, P., 1990. Elimination of cluster interferences in secondary ion mass spectrometry using extreme energy filtering. Int. J. Mass Spectrom. Ion Process. 103, 21–29.

Schauer, S.N., Williams, P., Hervig, R., Lareau, R.T., 1993. Energy dependent mass fractionation of ions during sputtering. SIMS 9, 64–67.

Sharp, Z.D., 1990. A laser based microanalytical method for the in situ determination of oxygen isotope ratios in silicates and oxides. Geochim. Cosmochim. Acta 54, 1353–1357.

Sharp, Z.D., Cerling, T.E., 1995. A laser GC–IRMS method for in situ carbon and oxygen isotope analysis of carbonates and phosphates. Geol. Soc. Am. Abstr. Prog. A 255.

Shimizu, N., Hart, S.R., 1982. Applications of the ion microprobe to geochemistry and cosmochemistry. Annu. Rev. Earth Planet. Sci. 10, 483–526.

Shroeer, J.M., Rhodin, T.N., Bradley, R.C., 1973. A quantum-mechanical model for the ionization and excitation of atoms during sputtering. Surface Sci. 34, 571–580.

Sigmund, P., 1969. Theory of sputtering, I. Sputtering yield of amorphous and polycrystalline targets. Phys. Rev. 184, 383–416.

Slodzian, G., Lorin, J.C., Havette, A., 1980. Isotopic effect on the ionization probabilities in secondary ion emission. J. Phys. 41, L555–L558.

Thompson, M.W., 1968. II. The energy spectrum of ejected atoms during the high energy sputtering of gold. Philos. Mag. 18, 377–414.

Valley, J.W., Graham, C.M., 1991. Ion microprobe analysis of oxygen isotope ratios in granulite facies magnetites: diffusive exchange as a guide to cooling history. Contrib. Mineral. Petrol. 109, 38–52.

Valley, J.W., Graham, C.M., 1996. Ion microprobe analysis of oxygen isotope ratios in quartz from Skye granite: healed micro-cracks, fluid flow, and hydrothermal exchange. Contrib. Mineral. Petrol. 124, 225–234.

Valley, J.W., Kitchen, N., Kohn, M.J., Niendorf, C.R., Spicuzza, M.J., 1995. UWG-2, a garnet standard for oxygen isotope ratio: strategies for high precision and accuracy with laser heating. Geochim. Cosmochim. Acta 59, 5223–5231.

Valley, J.W., Graham, C.M., Harte, B., Eiler, J.M., Kinny, P.D., 1997a. Ion microprobe analysis of oxygen, carbon and hydrogen isotope ratios. In: M.A. McKibben and W.C. Shanks (Editors), Applications of Microanalytical Techniques to Understanding Mineralizing Processes, Vol. 7, in press.

Valley, J.W., Kinny, P.D., Schulz, D.J. and Spicuzza, M.J., 1997b. Zircon megacrysts from kimberlite: O isotope heterogeneity in the mantle. Science, submitted.

Weathers, D.L., Spicklemire, S.J., Tombrello, T.A., Hutcheon, I.D., Gnaser, H., 1993. Isotopic fractionation in the sputtering of ^{92}Mo–^{100}Mo targets. Nucl. Instrum. Methods, B 73, 135–150.

Wiechert, U., Hoefs, J., 1995. An excimer laser-based micro analytical preparation technique for in situ oxygen isotope analysis of silicate and oxide minerals. Geochim. Cosmochim. Acta 59, 4093–4101.

Williams, P., 1979. The sputtering process and sputtered ion emission. Surf. Sci. 90, 588–643.

Yu, M.L., Lang, N., 1986. Mechanisms of atomic ion emission during sputtering. Nucl. Instrum. Methods B14, 403–413.

Yurimoto, H., Nagasawa, H., Mori, Y., Matsubaya, O., 1994. Micro-distribution of oxygen isotopes in a refractory inclusion from the Allende meteorite. Earth Planet. Sci. Lett. 128, 47–53.